

Signatures of gate-driven out of equilibrium superconductivity in Ta/InAs nanowires

Tosson Elalaily,^{1,2,3} Martin Berke,^{1,2} Máté Kedves,^{1,4} Gergő Fülöp,^{1,2} Zoltán Scherübl,^{1,2} Thomas Kanne,⁵ Jesper Nygård,⁵ Péter Makk,^{1,4,*} and Szabolcs Csonka^{1,2,†}

¹*Department of Physics, Institute of Physics, Budapest University of Technology and Economics, Műegyetem rkp. 3., H-1111 Budapest, Hungary*

²*MTA-BME Superconducting Nanoelectronics Momentum Research Group, Műegyetem rkp. 3., H-1111 Budapest, Hungary*

³*Department of Physics, Faculty of Science, Tanta University, Al-Geish St., 31527 Tanta, Gharbia, Egypt*

⁴*MTA-BME Correlated van der Waals Structures Momentum Research Group, Műegyetem rkp. 3., H-1111 Budapest, Hungary*

⁵*Center for Quantum Devices and Nano-Science Center, Niels Bohr Institute, University of Copenhagen, Universitetsparken 5, DK-2100, Copenhagen, Denmark*

Understanding the microscopic origin of the gate-controlled supercurrent (GCS) in superconducting nanobridges is crucial for engineering superconducting switches suitable for a variety of electronic applications. The origin of GCS is controversial, and various mechanisms have been proposed to explain it. In this work, we have investigated the GCS in a Ta layer deposited on the surface of InAs nanowires. Comparison between switching current distributions at opposite gate polarities and between the gate dependence of two opposite side gates with different nanowire–gate spacings shows that the GCS is determined by the power dissipated by the gate leakage. We also found a substantial difference between the influence of the gate and elevated bath temperature on the magnetic field dependence of the supercurrent. Detailed analysis of the switching dynamics at high gate voltages shows that the device is driven into the multiple phase slips regime by high-energy fluctuations arising from the leakage current.

INTRODUCTION

Since superconducting circuits have the potential to realize electronics with short switching time and ultra-low power consumption, various architectures have been developed for integrating semiconductor technology with superconducting devices to reduce the high power consumption required for cooling the high-density semiconductor-based microchips [1–3]. The cryotron [4], Josephson cryotron [5], rapid single flux quantum (RSFQ) device [6], and nanocryotron (nTron) [1] were all developed as building blocks for superconducting switches, however, their scalability or even the difficulty of interfacing with CMOS electronics limited their applications.

In the recent years, suppression of supercurrent by applying a voltage to a gate electrode in the vicinity of superconducting metallic nanowire has attracted much attention as a promising building block for highly scalable superconducting switches [7–28]. In some works, the effect is attributed to the large electric field (10^8 V/m) at the superconducting surface [7–21], which distorts the superconducting state and leads to the quenching of the superconductivity [29–33]. Other studies [22–28] reported a correlation between the gate controlled supercurrent (GCS) and the leakage current flowing between the gate and the superconducting device. Some of these studies suggest that the GCS results from ballistic injection of high-energy quasiparticles [24–26]. In another work, the quenching of the supercurrent was at-

tributed to the absorption of phonons emitted in the relaxation process of high-energy electrons injected from the gate electrode [28]. In order to engineer efficient superconducting switches for future electronic applications, it is important to understand the dominant mechanism behind the CGS effect.

In this work, we have studied the GCS in a superconducting Ta shell deposited on the surface of InAs nanowires [34]. We chose Ta because of its strong spin-orbit interaction [35, 36], so it is expected that the electric field has a strong influence on the superconducting state. We investigated the influence of the distance between the gate and the nanowire on the suppression of the supercurrent for the fabricated devices. Also, the magnetic field dependence of the supercurrent under the influence of the gate voltage and elevated temperatures was investigated. In addition, the switching current distribution at opposite gate polarities and at different current ramp speeds was studied. Furthermore, we give a detailed analysis for the switching dynamics at high gate voltages. Our findings contradict the proposed theoretical explanations based on electric fields or ballistic injection of high-energy electrons, and they are consistent with the nonequilibrium phonons picture as the origin of the GCS effect.

EXPERIMENTS

A. Device outline and characterization

In our device configuration, we used InAs nanowires with a 20-nm-thick Ta shell layer deposited on only three facets of the nanowire [34]. In order to investigate the

* makk.peter@ttk.bme.hu

† szabolcs.csonka@ttk.bme.hu

impact of the gate on the supercurrent flowing in the Ta layer, four-terminal nanowire-based devices were fabricated with the configuration shown in Fig. 1a, b. The Ta/InAs nanowires (green/brown) were deposited on a doped Si wafer with a 290-nm-thick oxide layer. Four Ti/Al contacts (blue) with a thickness of 10/80 nm were fabricated for quasi-four terminal measurements. A two metallic Ti/Au side gates SG1 (orange) and SG2 (light blue) with a thickness of 7/33 nm were placed with unequal spacings and on opposite sides of the nanowire. This provides a possibility to study the GCS effect for the device with gates at different spacings. The results presented in this paper are based on measurements performed on three different devices, A, B and C with the same device geometry, but with different values of nanowire–gate spacing d in the range from 30 to 120 nm. The results in Fig. 1 were measured on device A, in Fig. 2 on device B, while the results in Fig. 3 and their analysis in Fig. 4 were performed on device C.

The current–voltage ($I - V$) characteristics measured at 35 mK show a clear switching from the superconducting state to the normal state at the switching current $I_{SW} \simeq 1.17 \mu\text{A}$ (see blue curve in Fig. 1c). When the measurements are carried out in the opposite sweep direction (grey curve), the device shows a hysteretic behaviour and switches back to the superconducting state at two successive retrapping current values at $\simeq 0.61 \mu\text{A}$ and $0.4 \mu\text{A}$. This hysteretic behaviour can be attributed to large Joule heating dissipated in the resistive state [37]. The GCS is investigated by measuring the dependence of I_{SW} under the influence of gates SG1 (orange) and SG2 (light blue) with d of $\simeq 65$ and $\simeq 115$ nm, respectively. Fig. 1d shows I_{SW} as a function of V_{sg} for both gates, where each of the plotted curves has the same colour as the corresponding gate in Fig. 1a. The plot reveals that both gates completely switch the device to the normal state at almost the same critical gate voltage $V_{sg,C} \simeq \pm 13$ V. Despite the nanowire–gate spacing for SG1 is about half that for SG2, SG2 still suppresses I_{SW} at lower threshold gate voltage V_{th} than SG1. Importantly, at V_{th} , a correspondingly large increase in the gate leakage current I_{leak} is observed for each of the gates (see Fig. 1e), which has also been reported elsewhere [22, 23, 25, 26, 28].

B. Magnetic field dependence

The dependence of the supercurrent in our device on the out-of-plane magnetic field B is shown in Fig. 2a, where the $I - V$ curves are measured as a function of the B -field up to ± 2 T. The white region represents the zero-resistance state, with a transition to and from the normal state (red and blue regions) at the switching and retrapping current values in the positive and negative bias current values, respectively. The magnitude of I_{SW} shows a rapid suppression with increasing B -field below 100 mT and then slowly decreases with further increasing the magnetic field up to 2 T. The sharp decrease in the

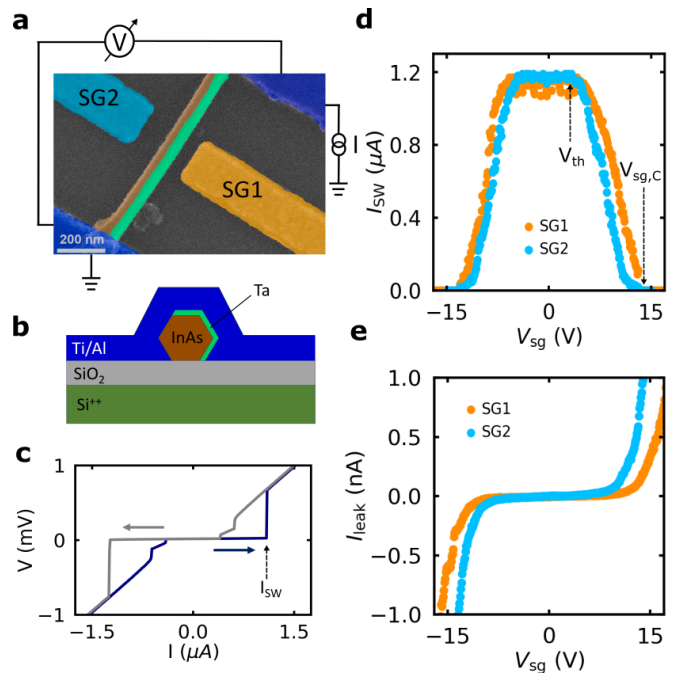


FIG. 1. **Device geometry and gate dependence characterization (Device A).** **a** A false-colored SEM image and **b** schematic of the side view of the nanowire device. **c** $I - V$ characteristics of the device measured at 35 mK. As the bias current ramps from negative to positive values (blue arrow), the device switches to finite-resistance state at the switching current $I_{SW} = 1.17 \mu\text{A}$. If the current ramps in the opposite direction (grey arrow), the device switches back to the superconducting state at two successive retrapping current values at $\simeq 0.61 \mu\text{A}$ and $\simeq 0.4 \mu\text{A}$. **d** I_{SW} as a function of V_{sg} (at magnetic field $B = 0.1$ T) applied to SG1 (orange curve) and SG2 (light blue curve) with nanowire–gate spacings of $\simeq 65$ and $\simeq 115$ nm, respectively. **e** The leakage current as a function of V_{sg} for both gates.

critical current below 100 mT coincides with the B_C of the Al electrodes contacting the nanowire [23], therefore we believe that this decrease is a result of the Al contacts switching to normal state. Although the maximum B -field in our setup (2 T) does not allow full suppression of the superconducting state in the Ta shell, based on the measured trend, B_C is expected to be about 3.5 T, which is consistent with earlier findings on identical Ta/InAs nanowires [38].

The gate dependence of I_{SW} under the influence of B -field is shown in Fig. 2b. I_{SW} is plotted as a function of V_{sg} at different values of magnetic field up to 2 T. No significant change in $V_{sg,C}$ with increasing B -field was observed, which is in contrast to the dependence observed for Ti and Al nanostructures [7, 23]. Fig. 2c and d show the dependence of I_{SW} on B -field under influence of temperature T and V_{sg} , respectively. In the former case, I_{SW} decreases with increasing T , as expected, accompanied by a suppression of B_C , giving $B_C = 2$ T at 800 mK and $B_C = 1.5$ T at 900 mK. In the case of the gate

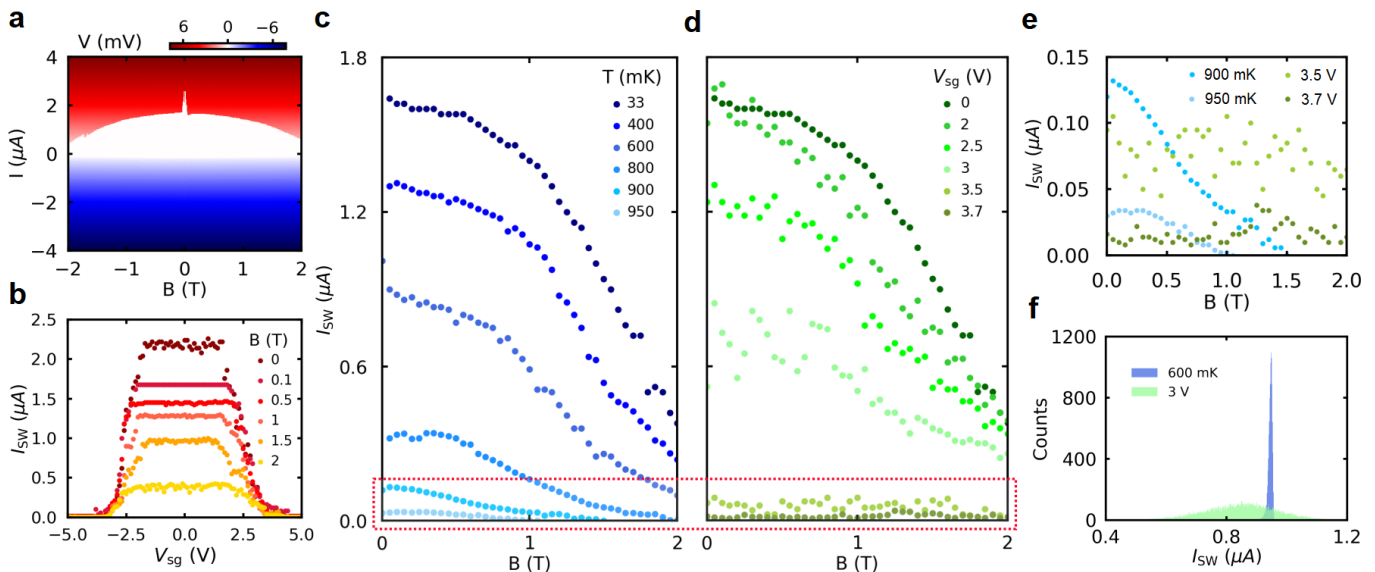


FIG. 2. **Magnetic field dependence and comparison between the GCS effect and effect of bath temperature (device B, $d = 35$ nm).** **a** $I - V$ curve as a function of out-of-plane magnetic field B up to ± 2 T. **b** I_{SW} as a function of V_{sg} at various values of B -field up to 2 T. **c** I_{SW} as a function of the B -field at various elevated temperatures and, **d** at various values of V_{sg} . **e** Magnification of the curves surrounded by the red rectangle in **c** and **d**. **f** Comparison between the SCDs measured at $T = 600$ mK (blue) and $V_{sg} = 3$ V (green).

control, I_{SW} also decreases with increasing V_{sg} , but surprisingly, *no change in B_C was observed*. For a better comparison, Figs. 2e shows a zoom in of the curves in both dependencies marked by the red rectangle and having almost the same magnitude of I_{SW} (at $B = 0$ T). It can be clearly seen that the B_C dependence behaves differently under the influence of temperature and gate voltage. While from 900 mK to 950 mK B_C further decreases from 1.5 T to 1 T, I_{SW} does not seem to be suppressed by the magnetic field in the case of the gate (see also the Supporting Information) in strong contradiction to other works [10, 16, 23].

Another remarkable difference between temperature and gate dependence is that I_{SW} exhibits large fluctuations at finite gate voltages (see green curves in Fig. 2e). In order to investigate this effect, the switching current distribution (SCD) at finite temperatures and gate voltages is measured by ramping the current at constant speed from 0 to $3 \mu\text{A}$ for 10,000 times and recording the corresponding I_{SW} value every time (see Methods). A comparison between the SCDs obtained at 600 mK and 3 V is shown in Fig. 2f. Despite the fact that both histograms have almost the same mean value $\langle I_{SW} \rangle$, the width of the histogram obtained under influence of the gate voltage is an order of magnitude larger than that obtained at elevated bath temperature. The large gate-induced broadening is consistent with Refs. 14, 19, 22, 26, 28 and shows that the gate voltage induces an out-of-equilibrium state in the superconducting nanowire, which cannot be described with an effective temperature.

C. Gate dependence of the probability distributions

In the following, we will compare the SCDs measured at positive and negative gate polarity, as they are expected to behave differently for different microscopic origins of the GCS. The dependence of I_{SW} on V_{sg} of the device is shown in the inset of Fig. 3a, where the positive and negative gate polarities represented by the orange and blue curves, respectively. Fig. 3a shows the SCDs measured at the same $|V_{sg}|$ but with opposite polarities are paired and shifted along the y-axis for clarity. For simplicity, we made the measurements with the Al leads in the normal state, at $B = 100$ mT [23]. There is a clear difference in the shape and $\langle I_{SW} \rangle$ of SCDs paired at equal $|V_{sg}|$. In addition, we also paired SCDs for opposite gate polarities and with approximately the same power dissipated at the gate $P_G = I_{leak} \cdot V_{sg}$ as shown in Fig. 3b. Comparing Fig. 3a and b, one can conclude that the pairing at the same power gives a better match between SCDs with opposite polarities. We also found that the SCDs measured at positive polarity have a slightly smaller $\langle I_{SW} \rangle$ than those measured at negative polarity at the same P_G (see inset in Fig. 3b).

Assuming that the electric field E applied by the gate (Fig. 3c) is responsible for the suppression of I_{SW} [29–33], its effect should not depend on the sign of E . Therefore, we expect the SCD obtained at a given voltage V_{sg} to be identical to the SCD obtained at the same gate voltage with the opposite sign, $-V_{sg}$. Since the measured SCDs do not match at opposite polarities (see Fig. 3a), our results contradict the electric field-based explanation. Another

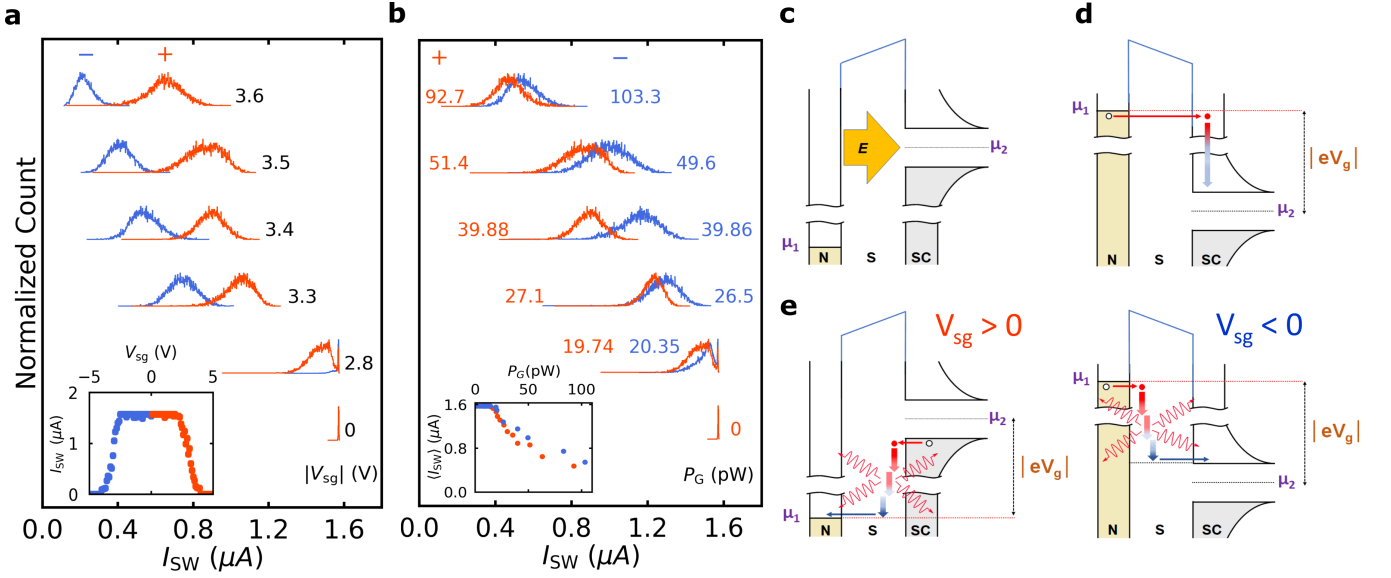


FIG. 3. **SCD measurements and schematics for different proposed mechanisms of the GCS effect (device C, $d = 30$ nm).** **a** SCDs measured at positive (orange) and negative (blue) gate polarity and paired at the same $|V_{sg}|$. The SCDs are normalized to their maximum counts and shifted on the y-axis for clarity. The inset shows I_{SW} as a function of V_{sg} for the investigated device measured at 0.1 T. **b** SCDs measured at positive (orange) and negative (blue) gate polarity and paired at approximately the same P_G . The inset shows the mean value of $\langle I_{SW} \rangle$ of SCDs measured at both gate polarities as a function of P_G . **c** Schematic diagram of the electric field E applied from the metallic gate N to the superconducting nanowire SC at positive gate polarity. The colored/uncolored parts represent occupied/unoccupied states. **d** Schematic diagram of the ballistic electron injection from the gate to the nanowire at negative gate polarity. The high-energy electron (red circle) tunnels through the potential barrier of the substrate S and relaxes to the lowest unoccupied state (close to the superconducting gap edge), releasing heat on the SC-side. **e** Schematic diagram of relaxation of high-energy electrons in the substrate when injected from the SC/N side to N/SC at positive/negative gate polarity in the left/right panels. In the case of positive gate polarity, the electrons relax close to the SC side (superconducting nanowire) so that it is heated more than in the case of negative gate polarity at the same P_G .

possible microscopic picture is that the CGS is caused by ballistic injection of high-energy quasiparticles, as shown in Fig. 3d. After injection of these electrons, their energy is released by relaxation, heating the side on which they end up. Therefore, for negative gate polarity (Fig. 3d), they heat the superconducting bridge, while for positive polarity they heat the gate electrode instead. Thus, a stronger suppression of superconductivity is expected for negative polarity. Therefore, at the same P_G value, the mean value of the distribution is expected to be significantly smaller for negative polarity than for positive polarity. Comparing this prediction with the measured results in Fig. 3b, one can conclude that the experimental findings are just opposite, so that ballistic injection of electrons can also be excluded.

The most likely explanation for our results is the generation of phonons by series of relaxation events of the high-energy electrons in the substrate [28]. The small shift between the $\langle I_{SW} \rangle$ measured for the two polarities (see Fig. 3b) can be attributed to the short energy relaxation length of electrons in SiO_2 (≤ 3 nm) at high electric fields compared to nanowire–gate spacing ($d = 30$ nm) [39–42]. Thus, at positive gate polarity, it is expected that the high-energy electrons will relax close to the nanowire (Fig. 3e, left panel) and the generated phonons can heat

the superconducting nanowire more than at negative gate polarity (Fig. 3e, right panel).

D. Analysis of the switching dynamics

The standard deviation σ of SCDs measured under the influence of the gate is represented by the blue curve in Fig. 4a. For small values of $|V_{sg}|$, where I_{leak} is negligible, σ is independent of $|V_{sg}|$ and no significant change in the $\langle I_{SW} \rangle$ of SCDs (green curve) was observed. Beyond V_{th} at $|V_{sg}| = 2.7$ V, σ increases with $|V_{sg}|$ because the fluctuations assisted by I_{leak} become stronger and more frequent. This increases the probability of nanowire switching at small I_{SW} values with a corresponding suppression in the $\langle I_{SW} \rangle$ of the SCD. This increase in the width of the SCDs is analogous to the typical temperature dependence (see the Supporting Information) [14, 19, 43] associated with thermally-activated phase slips [44, 45]. However, the large width of the SCDs obtained under the influence of the gate indicates that the system is driven to a nonequilibrium state where the fluctuations are an order of magnitude larger than expected from the bath temperature. With further increasing $|V_{sg}|$, σ decreases and

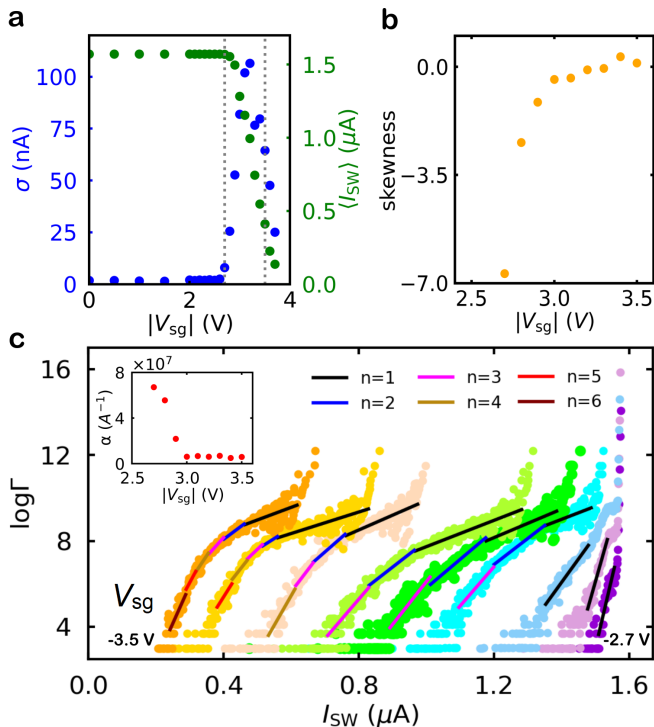


FIG. 4. **Analysis of the switching dynamics under influence of V_{sg} (device C, $d = 30$ nm).** **a** Standard deviation σ and mean value $\langle I_{\text{sw}} \rangle$ as a function of $|V_{\text{sg}}|$ for all SCDs measured at negative gate polarity in the blue and green curves, respectively. **b** The calculated skewness as a function of $|V_{\text{sg}}|$ for SCDs measured with a step of 0.1 V in the interval $[-3.5, -2.7$ V] (surrounded by the vertical grey dotted lines in panel a) where a corresponding increase in I_{leak} is observed. **c** Logarithm of escape rate Γ as a function of I_{sw} (colored curves) for different values of V_{sg} from -3.5 V (orange curve) up to -2.7 V (purple curve) with a step of 0.1 V. The colored solid lines represent the fitting of different portions of these curves with an exponential of higher orders n of the slope α . The inset shows the variation of the slope α with increasing V_{sg} .

the SCDs become more symmetric, as shown by their calculated skewness in Fig. 4b. This is analogous with the picture that the switching of the system is due to multiple phase slips (MPS) found at finite temperatures [43].

Interestingly, the SCD in Fig. 3a at $V_{\text{sg}} = 2.8$ V (orange curve) shows two peaks, a sharp one at $1.57 \mu\text{A}$ and a broad one around $1.5 \mu\text{A}$. This distribution looks like the sum of two overlapping probability distributions, similar to distributions shown in Refs. 14, 22. Since the probability distribution in this transition region depends strongly on the ramp speed of the bias current ν_I (see the Supporting Information), we could completely switch between the two distributions when the ramp speed was changed from 300 (at which the SCDs in Fig. 3 are measured) to $9.375 \mu\text{A/s}$. For a more accurate evaluation, it is better to transform the measured probability distributions into the speed-independent escape rate $\Gamma(I, T)$ (see

the Supporting Information) by the direct Kurkijärvi-Fulton-Dunkleberger (KFD) transformation [45–47]:

$$\Gamma(I_N, T) = \frac{P(I_N, T)\nu_I}{1 - w \sum_{k=0}^N P(I_k, T)} \quad (1)$$

where w is the bin size in the current axis of the measured probability distribution $P(I, T)$, and $P(I_k, T)$ is the switching probability in the bias current interval $[kw, (k+1)w]$ with $k \in [0, N]$. Fig. 4c shows the logarithm of the calculated $\Gamma(I_N, T)$ as a function of current for SCDs measured under the influence of V_{sg} in the interval $[-3.5, -2.7$ V]. As long as V_{sg} is small, the SCDs have a sharp peak around $I_{\text{sw}} = 1.57 \mu\text{A}$, resulting in a large escape rate around this value, which represents the escape rate due to quantum tunnelling or thermal escape Γ_T . As the influence of the gate voltage sets in (see e.g., purple curve), a finite escape rate appears at lower I_{sw} values, corresponding to the gate-assisted escape rate Γ_L . The latter contribution becomes the dominant escape rate at higher gate voltages (see e.g., green curve).

For $V_{\text{sg}} > -3$ V, where I_{leak} is negligible (the first three curves from the right), Γ_L can be well fitted with an exponential curve (black solid line) given by

$$\Gamma_L(I_{\text{sw}}) = Ae^{n\alpha I_{\text{sw}}} \quad (2)$$

with $n = 1$ and using α and A as fitting parameters. The switching dynamics in this region have been studied in detail in Ref. 22. On the other hand, for $V_{\text{sg}} \leq -3$ V Γ_L deviates from the single exponential dependence described by Eq. 2. For example, the light green curve measured at -3.2 V can be fitted at large current values using Eq. 2 with $n=1$ (see black solid lines). Interestingly, the measured curve for $I_{\text{sw}} < 0.9 \mu\text{A}$ can be well fitted by adding extra higher order terms with $n=2, 3, \dots$, keeping the same values of the fitting parameters. Further increasing V_{sg} (I_{leak}) requires more higher order terms to fit the escape rate dependence (e.g. orange curve) [43]. The value of α required to fit the escape rate dependence decreases sharply as V_{sg} increases, and saturates at large values of V_{sg} as shown in the inset of Fig. 3c.

The deviation of the escape rate dependence with current from a pure exponential at higher gate voltages is similar to elevated temperatures in Ref. 43. This can be attributed to the reduced impact for a single fluctuation event triggered by the leakage current, since the dissipation during the induced phase slip event is smaller at lower values of I_{sw} [43, 45]. Thus, several coincident fluctuation events with corresponding induced multiple phase slips (MPS) are required to trigger the switching of the nanowire to the normal state [43, 48, 49]. In this regime, at large bias current values, the dissipation of a single MPS event ($n = 1$) is sufficient to switch the nanowire into the resistive state. On the other hand, at lower current values, the dissipation of a single MPS event is reduced and higher orders ($n = 2, 3, \dots$) of the

MPS event are required to trigger the resistive switching of the nanowire [43].

COMPARISON WITH THE PROPOSED MICROSCOPIC PICTURES

In the following, we will compare our experimental results with the possible microscopic pictures. Starting from the two gates (Fig. 1d,e), despite SG2 has almost twice the nanowire–gate spacing of SG1, it suppresses the I_{SW} at lower V_{th} than SG1. This contradicts the electric field picture as a possible explanation for the origin of the GCS. On the other hand, I_{SW} starts to be suppressed with the onset of leakage current between the nanowire and each of the gates (see the Supporting Information). In another cool-down, the influence of the two gates for the same device shows an opposite situation, as SG1 shows a stronger influence on I_{SW} than SG2 (see the supporting information). This excludes any concerns arising from the quite large dielectric constant of the InAs nanowire between SG2 and the Ta shell (see Fig. 1a), which may lead to a larger influence of SG2 on I_{SW} than SG1. Interestingly, we found that the influence of the two gates on I_{SW} gives better matching with P_G in the two cool-downs (see the Supporting Information).

Accepting that the leakage current plays a key role in the GCS, a simple explanation arises: that the leaking electrons increase the temperature of the superconducting nanowire. We have investigated for the first time the B -field dependence of superconducting nanowire with normal contacts, which allows efficient cooling of the superconducting nanowire. The B -field dependence at finite T and finite gate voltage was strictly different, indicating that the effect of leakage current cannot be described by simple hot electron regime induced by elevated bath temperature. The highly non-equilibrium state of the superconductor at finite gate voltage is further supported by the broad SCDs in our work and in previous results [14, 19, 22, 26, 28]. Our detailed comparison of the SCDs for different gate polarities (Fig. 3) provided another important finding which is inconsistent with electric-field-induced suppression of superconductivity. Pairing of SCDs measured at opposite gate polarities at the same leakage current dissipation, P_G , provided a better matching than at the same $|V_{sg}|$ (Fig. 3a,b). This reveals that the suppression of I_{SW} depends not only on the energy of the injected electrons (eV_{sg}) or the rate of their injection (I_{leak}/e), but on the power dissipated at the gate P_G . Based on the $\langle I_{SW} \rangle$ of the SCDs for the two polarities, the ballistic injection of electrons from the gate into the superconducting nanowire can be discarded. We conclude that the phonon-mediated excitation of the superconductor remains a microscopic picture consistent with the measured results.

Furthermore, we also noticed that the power dissipation at the gate required to fully suppress I_{SW} , $P_{G,C}$ is comparable to the power dissipation that occurs when

the device switches to the resistive state $P_n = I_{SW}^2 \cdot R_n$. For example, for device A, in the case of SG1 (the closer to the Ta shell), $P_{G,C} \simeq 1.5$ nW (see the Supporting Information), while $P_n \simeq 1$ nW (using $R_n = 780 \Omega$ and $I_{SW} \simeq 1.17 \mu A$).

Finally, a very large leakage current was required to quench I_{SW} when we investigated the GCS in similar Ta/InAs devices fabricated on a sapphire substrate (see the Supporting Information). These results indicate that the GCS depends mainly on the properties of the substrate and the leakage pathway between the gate and nanowire.

CONCLUSIONS

We investigated the origin of GCS in the Ta half-shell layer deposited on InAs nanowires by various measurements. Devices with small nanowire-gate spacing (specifically devices B and C) fully switch to the normal state below $V_{sg} = \pm 5$ V, which makes them promising for integration into classical electronic circuits. When the wire is connected by electrodes in the normal state, the critical magnetic field B_C is not suppressed under the influence of the gate as for elevated temperatures. Moreover, the comparison of the switching current distributions at opposite gate polarities, as well as the gate dependence of two opposite side gates at different nanowire-gate spacings show that the power dissipated at the gate P_G is the relevant parameter for this effect. Analysis of the switching dynamics under strong gate influence shows a deviation in the escape rate dependence with the bias current from a pure exponential. This indicates that the device is driven into the MPS regime by the high energy fluctuations originating from the leakage current. Our findings contradict the microscopic pictures proposing electric fields or ballistic injection of high-energy electrons as the origin of the GCS effect, but they are consistent with the non-equilibrium superconducting state resulting from the absorption of phonons generated by the leakage current.

METHODS

InAs nanowires were grown by the VLS mechanism using Molecular Beam Epitaxy and the Ta shell was deposited in-situ under UHV using electron beam evaporation at a substrate temperature of about 25° C. Based on the TEM characterization, the morphology of the Ta shells was continuous but granular on the InAs nanowires and was found to be non-crystalline [38].

The Ta/InAs nanowires were deposited on the top of a doped Si wafer with 290 nm thick SiO₂ layer by means of a hydraulic micromanipulator along with a high magnification optical microscope. The nanowire device was fabricated in two separate electron beam lithography (EBL) steps. In the first step, four Ti/Al contacts with a thick-

ness of 10/80 nm were fabricated. Prior to the metal evaporation, Ta/InAs nanowires were exposed to Ar-ion plasma milling for 8 minutes at 50 W to remove any oxides on the top of the Ta shell. In the second step, two metallic gates of Ti/Au layers with a thickness of 7/33 nm were fabricated with unequal spacing and on opposite sides of the nanowire. The metallic gates were fabricated in a separate lithography step, since thin resist is used for precise alignment of the gates from the nanowire.

The $I - V$ characteristics of the device were measured by a pure DC measurements using a quasi 4-probe method in which the current was injected through the nanowire via a pair of Al contacts by using a standard voltage source (Basel DAC SP 927) with series resistor of 1 M Ω , while the voltage was measured across the other pair with a differential voltage amplifier and a digital multimeter (Keithley 2001). The leakage current was recorded by measuring the voltage across a 10 M Ω pre-resistor connected to the gate and corrected according to the method reported in Ref. 23.

The SCD was measured using a NI-DAQ card (USB-6341), where a periodic current wave signal was engineered. This signal is composed of a positive linear ramp with an amplitude of 3 μ A and a slope in the range from 9.375 to 300 μ A/s followed by a 2.5 ms of zero-current plateau for cooling down the superconducting device. This signal is repeated 10,000 times, and I_{SW} is extracted each time. All SCDs are measured at 0.1 T to switch the Al leads to the normal state. All measurements were carried out in a Leiden Cryogenics CF-400 top-loading cryo-free dilution refrigerator system with a

base temperature of 30 mK.

AUTHOR CONTRIBUTIONS

T.E., M.B. fabricated the devices, T.E., M.B., M.K., G.F. and Z.S. performed the measurements and did the data analysis. T. K. and J. N. developed the nanowires. All authors discussed the results and worked on the manuscript. P.M. and S.C. guided the project.

ACKNOWLEDGMENTS

This work has received funding from Topograph FlagERA, the SuperTop QuantERA network, SuperGate Fet Open, the FET Open AndQC, and from the OTKA FK-123894 grants. This research was supported by the Ministry of Innovation and Technology and the National Research, Development and Innovation Office within the Quantum Information National Laboratory of Hungary and by the Quantum Technology National Excellence Program (Project Nr. 2017-1.2.1-NKP-2017-00001), by the ÚNKP-22-5 New National Excellence Program, the János Bolyai Research Scholarship of the Hungarian Academy of Sciences, by ÚNKP-22-2-I-BME-22 New National Excellence Program of the Ministry for Culture and Innovation from the source of the National Research, Development and Innovation Fund, by the Carlsberg Foundation, Innovation Fund Denmark and the Danish National Research Foundation. We thank M. Bjergfelt, D. Carrad and T.S. Jespersen for their contributions to the development of the hybrid nanowires.

-
- [1] A. N. McCaughan and K. K. Berggren, "A superconducting-nanowire three-terminal electrothermal device," *Nano letters* **14**, 5748–5753 (2014).
 - [2] A. N. McCaughan, V. B. Verma, S. M. Buckley, J. Allmaras, A. Kozorezov, A. Tait, S. Nam, and J. Shainline, "A superconducting thermal switch with ultrahigh impedance for interfacing superconductors to semiconductors," *Nature electronics* **2**, 451–456 (2019).
 - [3] S. Frasca and E. Charbon, "Hybrid superconductor–semiconductor electronics," *Nature Electronics* **2**, 433–434 (2019).
 - [4] D. A. Buck, "The cryotron—a superconductive computer component," *Proceedings of the IRE* **44**, 482–493 (1956).
 - [5] J. Matisoo, "Subnanosecond pair-tunneling to single-particle tunneling transitions in josephson junctions," *Applied Physics Letters* **9**, 167–168 (1966).
 - [6] K. K. Likharev and V. K. Semenov, "Rsfq logic/memory family: A new josephson-junction technology for subterahertz-clock-frequency digital systems," *IEEE Transactions on Applied Superconductivity* **1**, 3–28 (1991).
 - [7] G. De Simoni, F. Paolucci, P. Solinas, E. Strambini, and F. Giazotto, "Metallic supercurrent field-effect transistor," *Nature nanotechnology* **13**, 802–805 (2018).
 - [8] G. De Simoni, F. Paolucci, C. Puglia, and F. Giazotto, "Josephson field-effect transistors based on all-metallic al/cu/al proximity nanojunctions," *ACS nano* **13**, 7871–7876 (2019).
 - [9] F. Paolucci, G. De Simoni, P. Solinas, E. Strambini, C. Puglia, N. Ligato, and F. Giazotto, "Field-effect control of metallic superconducting systems," *AVS Quantum Science* **1**, 016501 (2019).
 - [10] F. Paolucci, G. De Simoni, P. Solinas, E. Strambini, N. Ligato, P. Virtanen, A. Braggio, and F. Giazotto, "Magnetotransport experiments on fully metallic superconducting dayem-bridge field-effect transistors," *Physical Review Applied* **11**, 024061 (2019).
 - [11] F. Paolucci, F. Vischi, G. De Simoni, C. Guarcello, P. Solinas, and F. Giazotto, "Field-effect controllable metallic josephson interferometer," *Nano Letters* **19**, 6263–6269 (2019).
 - [12] G. De Simoni, C. Puglia, and F. Giazotto, "Niobium dayem nano-bridge josephson gate-controlled transistors," *Applied Physics Letters* **116**, 242601 (2020).
 - [13] M. Rocci, G. De Simoni, C. Puglia, D. D. Esposti, E. Strambini, V. Zannier, L. Sorba, and F. Giazotto, "Gate-controlled suspended titanium nanobridge super-

- current transistor,” *ACS nano* **14**, 12621–12628 (2020).
- [14] C. Puglia, G. De Simoni, and F. Giazotto, “Electrostatic control of phase slips in ti josephson nanotransistors,” *Physical Review Applied* **13**, 054026 (2020).
- [15] C. Puglia, G. De Simoni, N. Ligato, and F. Giazotto, “Vanadium gate-controlled josephson half-wave nanorectifier,” *Applied Physics Letters* **116**, 252601 (2020).
- [16] L. Bours, M. T. Mercaldo, M. Cuoco, E. Strambini, and F. Giazotto, “Unveiling mechanisms of electric field effects on superconductors by a magnetic field response,” *Physical Review Research* **2**, 033353 (2020).
- [17] C. Puglia, G. De Simoni, and F. Giazotto, “Gate control of superconductivity in mesoscopic all-metallic devices,” *Materials* **14**, 1243 (2021).
- [18] G. De Simoni, S. Battisti, N. Ligato, M. T. Mercaldo, M. Cuoco, and F. Giazotto, “Gate control of the current–flux relation of a josephson quantum interferometer based on proximitized metallic nanojunctions,” *ACS Applied Electronic Materials* **3**, 3927–3935 (2021).
- [19] C. PUGLIA, G. De Simoni, and F. Giazotto, “Phase slips dynamics in gated ti and v all-metallic supercurrent nano-transistors,” *Journal of Physics D: Applied Physics* (2021).
- [20] P. Orús, V. M. Fomin, J. M. De Teresa, and R. Córdoba, “Critical current modulation induced by an electric field in superconducting tungsten-carbon nanowires,” *Scientific Reports* **11**, 1–9 (2021).
- [21] F. Paolucci, F. Crisá, G. De Simoni, L. Bours, C. Puglia, E. Strambini, S. Roddaro, and F. Giazotto, “Electrostatic field-driven supercurrent suppression in ionic-gated metallic superconducting nanotransistors,” *Nano letters* **21**, 10309–10314 (2021).
- [22] J. Basset, O. Stanisavljević, M. Kuzmanović, J. Gabelli, C. Quay, J. Estève, and M. Aprili, “Gate-assisted phase fluctuations in all-metallic josephson junctions,” *Physical Review Research* **3**, 043169 (2021).
- [23] T. Elalaily, O. Kürtössy, Z. Scherübl, M. Berke, G. Fülöp, I. E. Lukács, T. Kanne, J. Nygård, K. Watanabe, T. Taniguchi, P. Makk, and S. Csonka, “Gate-controlled supercurrent in epitaxial al/inas nanowires,” *Nano letters* **21**, 9684–9690 (2021).
- [24] L. D. Alegria, C. G. Böttcher, A. K. Saydjari, A. T. Pierce, S. H. Lee, S. P. Harvey, U. Vool, and A. Yacoby, “High-energy quasiparticle injection into mesoscopic superconductors,” *Nature Nanotechnology* , 1–5 (2021).
- [25] M. Ritter, A. Fuhrer, D. Haxell, S. Hart, P. Gumann, H. Riel, and F. Nichele, “A superconducting switch actuated by injection of high-energy electrons,” *Nature communications* **12**, 1–6 (2021).
- [26] I. Golokolenov, A. Guthrie, S. Kafanov, Y. A. Pashkin, and V. Tsepelin, “On the origin of the controversial electrostatic field effect in superconductors,” *Nature Communications* **12**, 1–7 (2021).
- [27] G. Catto, W. Liu, S. Kundu, V. Lahtinen, V. Vesterinen, and M. Möttönen, “Microwave response of a metallic superconductor subject to a high-voltage gate electrode,” *arXiv preprint arXiv:2105.08322* (2021).
- [28] M. Ritter, N. Crescini, D. Haxell, M. Hinderling, H. Riel, C. Bruder, A. Fuhrer, and F. Nichele, “Out-of-equilibrium phonons in gated superconducting switches,” *Nature Electronics* **5**, 71–77 (2022).
- [29] M. T. Mercaldo, P. Solinas, F. Giazotto, and M. Cuoco, “Electrically tunable superconductivity through surface orbital polarization,” *Physical Review Applied* **14**, 034041 (2020).
- [30] M. T. Mercaldo, F. Giazotto, and M. Cuoco, “Spectroscopic signatures of gate-controlled superconducting phases,” *Physical Review Research* **3**, 043042 (2021).
- [31] P. Solinas, A. Amoretti, and F. Giazotto, “Sauter-schwinger effect in a bardeen-cooper-schrieffer superconductor,” *Physical Review Letters* **126**, 117001 (2021).
- [32] L. Chirrolli, T. Cea, and F. Giazotto, “Impact of electrostatic fields in layered crystalline bcs superconductors,” *Physical Review Research* **3**, 023135 (2021).
- [33] A. Amoretti, D. K. Brattan, N. Magnoli, L. Martinoia, I. Matthaiakakis, and P. Solinas, “Destroying superconductivity in thin films with an electric field,” *arXiv preprint arXiv:2202.00687* (2022).
- [34] D. J. Carrad, M. Bjergfelt, T. Kanne, M. Aagesen, F. Krizek, E. M. Fiordaliso, E. Johnson, J. Nygård, and T. S. Jespersen, “Shadow epitaxy for in situ growth of generic semiconductor/superconductor hybrids,” *Advanced Materials* **32**, 1908411 (2020).
- [35] Y. Niimi and Y. Otani, “Reciprocal spin hall effects in conductors with strong spin–orbit coupling: a review,” *Reports on progress in physics* **78**, 124501 (2015).
- [36] S. Vélez, V. N. Golovach, A. Bedoya-Pinto, M. Isasa, E. Sagasta, M. Abadia, C. Rogero, L. E. Hueso, F. S. Bergeret, and F. Casanova, “Hanle magnetoresistance in thin metal films with strong spin-orbit coupling,” *Physical review letters* **116**, 016603 (2016).
- [37] H. Courtois, M. Meschke, J. Peltonen, and J. P. Pekola, “Origin of hysteresis in a proximity josephson junction,” *Physical review letters* **101**, 067002 (2008).
- [38] M. Bjergfelt, *In-situ patterned superconductor/semiconductor nanowires for quantum devices*, Ph.D. thesis, FACULTY OF SCIENCE PhD thesis Martin Bjergfelt In-situ patterned . . . (2019).
- [39] Fischetti, M. V, DiMaria, D. J, Brorson, SD, Theis, TN, Kirtley, and JR, “Theory of high-field electron transport in silicon dioxide,” *Physical Review B* **31**, 8124 (1985).
- [40] S. Brorson, D. J. DiMaria, M. V. Fischetti, F. Pesavento, P. Solomon, and D. Dong, “Direct measurement of the energy distribution of hot electrons in silicon dioxide,” *Journal of applied physics* **58**, 1302–1313 (1985).
- [41] M. V. Fischetti, D. J. DiMaria, L. Dori, J. Batey, E. Tierney, and J. Stasiak, “Ballistic electron transport in thin silicon dioxide films,” *Physical Review B* **35**, 4404 (1987).
- [42] D. DiMaria and M. Fischetti, “Vacuum emission of hot electrons from silicon dioxide at low temperatures,” *Journal of applied physics* **64**, 4683–4691 (1988).
- [43] M. Ejrnaes, D. Salvoni, L. Parlato, D. Massarotti, R. Caruso, F. Tafuri, X. Yang, L. You, Z. Wang, G. Pepe, *et al.*, “Superconductor to resistive state switching by multiple fluctuation events in nbtin nanostrips,” *Scientific reports* **9**, 1–6 (2019).
- [44] D. McCumber and B. Halperin, “Time scale of intrinsic resistive fluctuations in thin superconducting wires,” *Physical Review B* **1**, 1054 (1970).
- [45] A. Bezryadin, *Superconductivity in Nanowires: Fabrication and Quantum Transport* (John Wiley & Sons, 2013).
- [46] J. Kurkijärvi, “Intrinsic fluctuations in a superconducting ring closed with a josephson junction,” *Physical Review B* **6**, 832 (1972).
- [47] T. Fulton and L. Dunkleberger, “Lifetime of the zero-voltage state in josephson tunnel junctions,” *Physical Review B* **9**, 4760 (1974).

- [48] N. Shah, D. Pekker, and P. M. Goldbart, "Inherent stochasticity of superconductor-resistor switching behavior in nanowires," *Physical review letters* **101**, 207001 (2008).
- [49] D. Pekker, N. Shah, M. Sahu, A. Bezryadin, and P. M. Goldbart, "Stochastic dynamics of phase-slip trains and superconductive-resistive switching in current-biased nanowires," *Physical Review B* **80**, 214525 (2009).

Signatures of gate-driven out of equilibrium superconductivity in Ta/InAs nanowires

Tosson Elalaily,^{1,2,3} Martin Berke,^{1,2} Máté Kedves,^{1,4} Gergő Fülöp,^{1,2} Zoltán Scherübl,^{1,2}
Thomas Kanne,⁵ Jesper Nygård,⁵ Péter Makk,^{1,4,*} and Szabolcs Csonka^{1,2,†}

¹*Department of Physics, Institute of Physics,
Budapest University of Technology and Economics,
Műegyetem rkp. 3., H-1111 Budapest, Hungary*

²*MTA-BME Superconducting Nanoelectronics Momentum Research Group,
Műegyetem rkp. 3., H-1111 Budapest, Hungary*

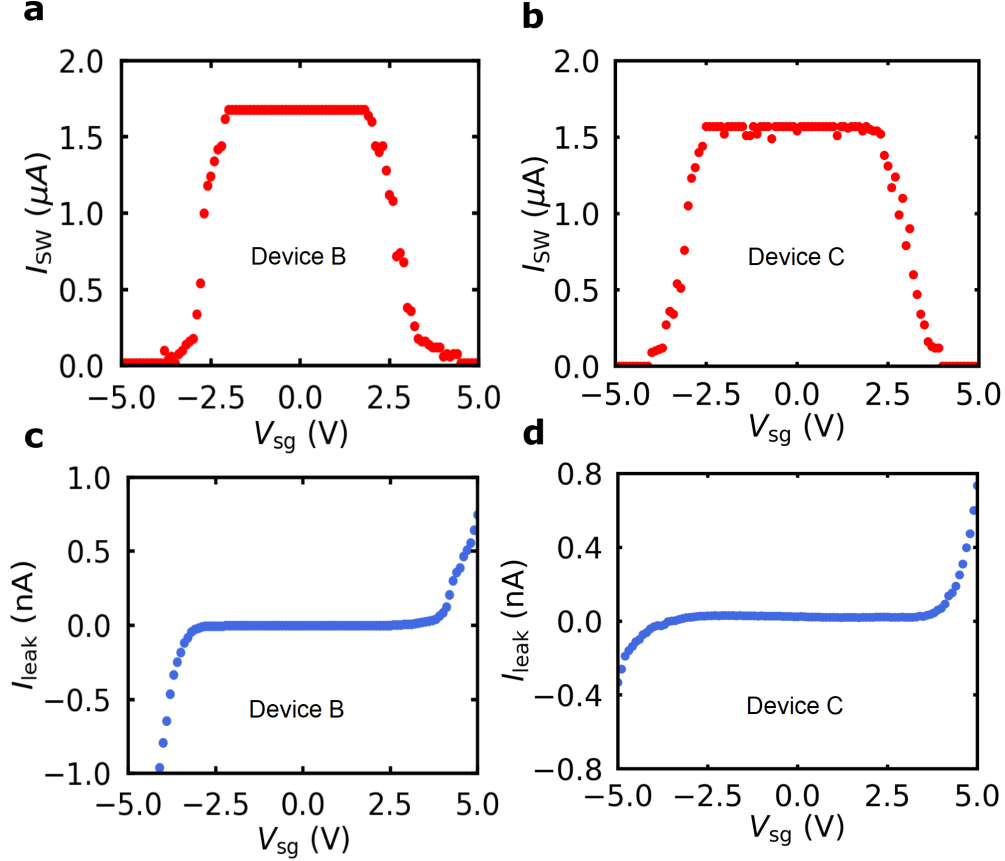
³*Department of Physics , Faculty of Science,
Tanta University, Al-Geish St., 31527 Tanta, Gharbia, Egypt*

⁴*MTA-BME Correlated van der Waals Structures Momentum Research Group,
Műegyetem rkp. 3., H-1111 Budapest, Hungary*

⁵*Center for Quantum Devices and Nano-Science Center,
Niels Bohr Institute, University of Copenhagen,
Universitetsparken 5, DK-2100, Copenhagen, Denmark*

I. GATE DEPENDENCE OF THE SUPERCURRENT FOR DEVICES B AND C

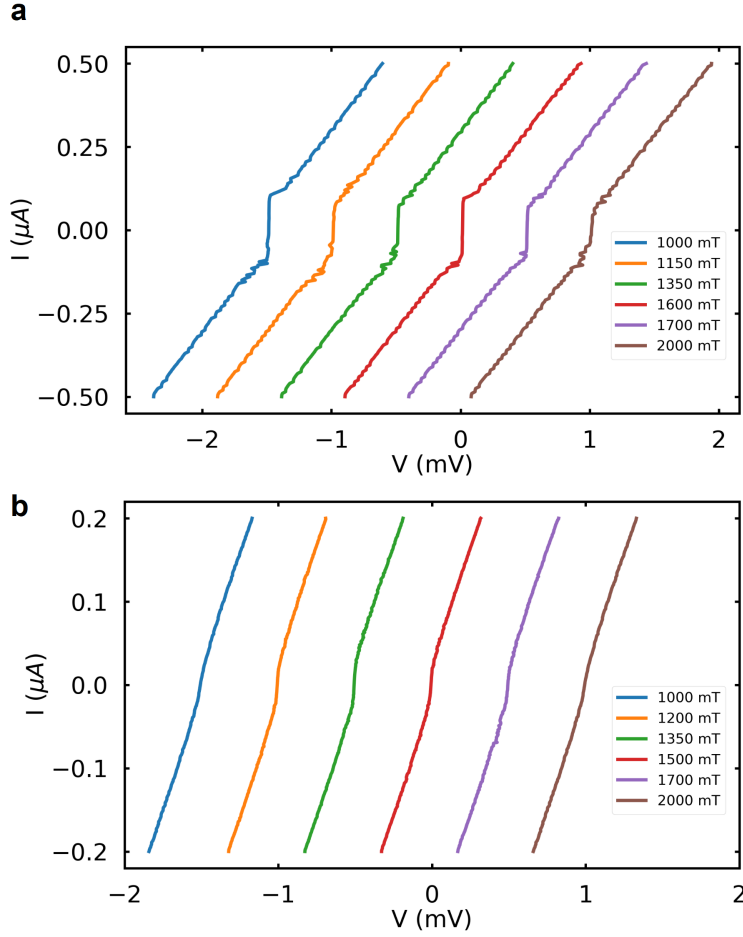
SFig. 1a and b show the I_{SW} as a function of V_{sg} for devices B and C, respectively. The gate dependence of the devices was investigated by using SG1 (the closest to Ta shell) at $B = 0.1$ T. Panels c and d show the corresponding I_{leak} as a function of V_{sg} .



SFig. 1. **a,b** I_{SW} as a function of V_{sg} for devices B and C at $B = 0.1$ T and their corresponding leakage current in **c,d**, respectively.

II. MAGNETIC FIELD DEPENDENCE UNDER INFLUENCE OF THE GATE

In the main text (see Fig. 2e), we compared the B -field dependence of the supercurrent of device B at finite temperature and finite gate voltage (with similar I_{SW} at $B = 0$ T). We found that B_{C} decreases with increasing temperature, but not with increasing V_{sg} . SFig. 2a,b shows some selected (I-V) curves at different B -field values ≥ 1 T at $V_{\text{sg}} = 3.5$ V and 3.7 V, respectively, separated in the x-axis for clarity.

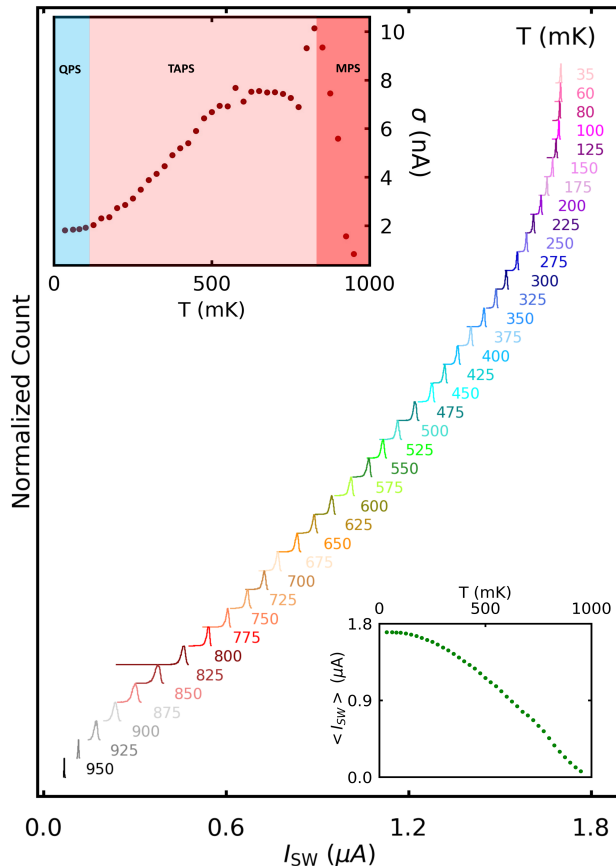


SFig. 2. **a** Selected (I-V) curves at different B -field values ≥ 1 T at $V_{\text{sg}} = 3.5$ V and **b** at $V_{\text{sg}} = 3.7$ V.

III. TEMPERATURE DEPENDENCE OF SCD

The dependence of SCDs measured at elevated temperatures for device B is shown in SFig. 3, in which SCDs measured at different temperatures at $B = 0.1$ T and normalized to their maximum count are plotted and separated on the y-axis for clarity. The corresponding standard deviation σ and mean value $\langle I_{\text{SW}} \rangle$ are plotted as a function of temperature T in the top left and bottom right insets, respectively.

The standard deviation σ follows the expected conventional dependence as a function of T (see Refs. ? ?), which can be divided into three distinct regions (different colored regions in the upper left inset) where the switching mechanism is attributed to quantum phase slips (QPS), thermally activated phase slips (TAPS), and multiple phase slips (MPS). Saturation of the width at the lowest temperatures can also originate from non-ideal thermalization of



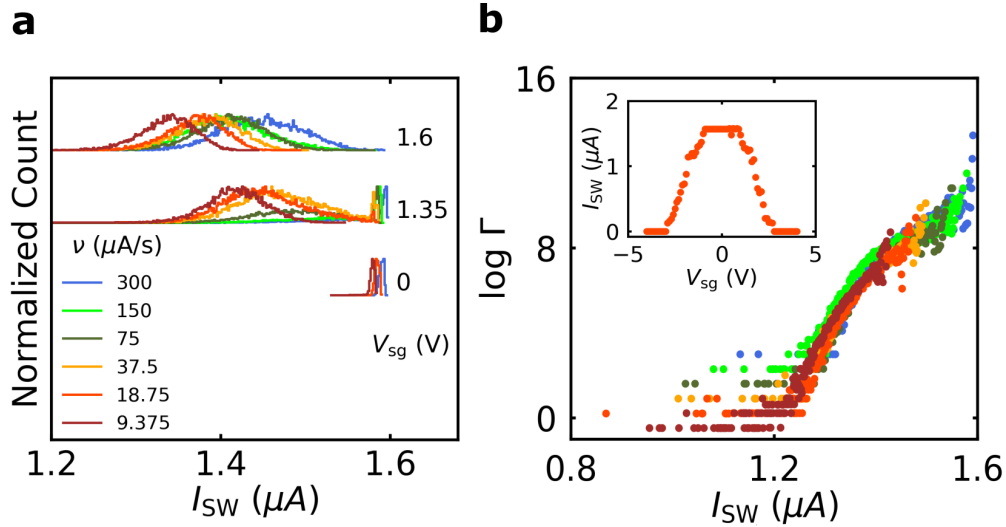
SFig. 3. Temperature dependence of SCDs for device C. In the top left, the standard deviation σ of the SCDs is plotted as a function of temperature. The colored regions represent the quantum phase slips (QPS) regime (light blue), the thermally activated phase slips (TAPS) regime (pink), and the multiple phase slips (MPS) regime (orange-red). In the bottom right inset, the $\langle I_{SW} \rangle$ of the SCDs is plotted as a function of temperature T .

the electron bath, in which case this could still be part of the TAPS regime. Since this will not play an important role in our analysis, we will refer to this regime as the QPS regime for simplicity.

IV. DEPENDENCE OF SCD AND ESCAPE RATE ON THE CURRENT RAMP SPEED

In this section, we discuss the dependence of SCDs on the current ramp speed ν_I for device C in another cool-down in which the gate dependence of I_{SW} is changed (V_{th} and

$V_{\text{sg,C}}$) compared to that in the main text as shown in the inset of SFig. 4b. SFig. 4a shows the SCDs measured at three different values of V_{sg} , and for each value they are measured at six different values of the current ramp speed ν_1 . The values of V_{sg} are chosen so that the measured SCDs are at the beginning (0 V), within (1.35 V), and at the end (1.6 V) of the transition region between quantum tunneling (or thermal activation) and leakage-assisted phase slips.

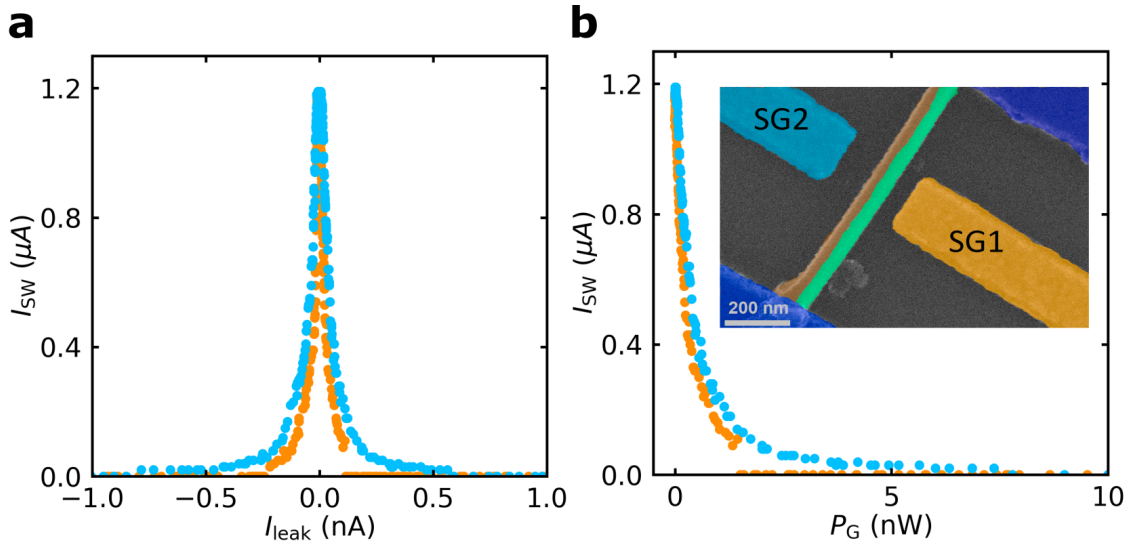


SFig. 4. **a** For device C, the SCDs were measured at $V_{\text{sg}} = 0, 1.35, 1.6$ V, and for each value they were measured at different current ramp speeds ν_1 . The SCDs are normalized by their maximum number of counts and separated on the y-axis. **b** Logarithm of escape rate Γ as a function of I_{SW} at different current ramp speeds ν_1 for SCDs measured at $V_{\text{sg}} = 1.6$ V.

At infinitely high values of ν , the superconductor is expected to have no time to switch prematurely in the presence of external fluctuations, and it will switch at $I_{\text{SW}} = I_C$, at which the system prefers to set at the lower energy of the normal state[?]. Thus, when ν_1 increases from 9.375 to 300 $\mu\text{A/s}$, the $\langle I_{\text{SW}} \rangle$ of the histograms shifts to higher current values, as shown in SFig. 4a. Interestingly, the SCD e.g. at 1.35 V appears as two overlapping probability distributions, where a complete switch between the two distributions depends on the value of ν_1 . Despite the SCDs depend strongly on ν_1 , the transformation of the measured probability distributions into the escape rate $\Gamma(I, T)$ is independent of ν_1 [?]. The transformed $\Gamma(I, T)$ for $V_{\text{sg}} = 1.6$ V evaluated from SCDs with different speeds are plotted in SFig. 4b.

V. COMPARISON BETWEEN THE INFLUENCE OF TWO OPPOSITE SIDE GATES FOR DEVICE A

Fig.1d and e in the main text show the dependence of I_{SW} on V_{sg} and the corresponding I_{leak} as a function of V_{sg} for two opposite side gates (SG1 and SG2) for device A. From these data, a parametric curve is plotted between I_{SW} and I_{leak} for the two gates in SFig. 5a. The plot shows that I_{SW} is suppressed for both gates at the onset of I_{leak} , despite it decreases at different V_{th} . A larger I_{leak} is required to switch the device to the normal state at negative gate polarity than at the opposite polarity. Plotting I_{SW} as a function of P_G as shown in SFig. 5b, a better matching between the two curves is observed. We also noticed that for SG1, $P_{G,C}$ is around 1.5 nW which is comparable to the switching power of the device $P_n \simeq 1$ nW.

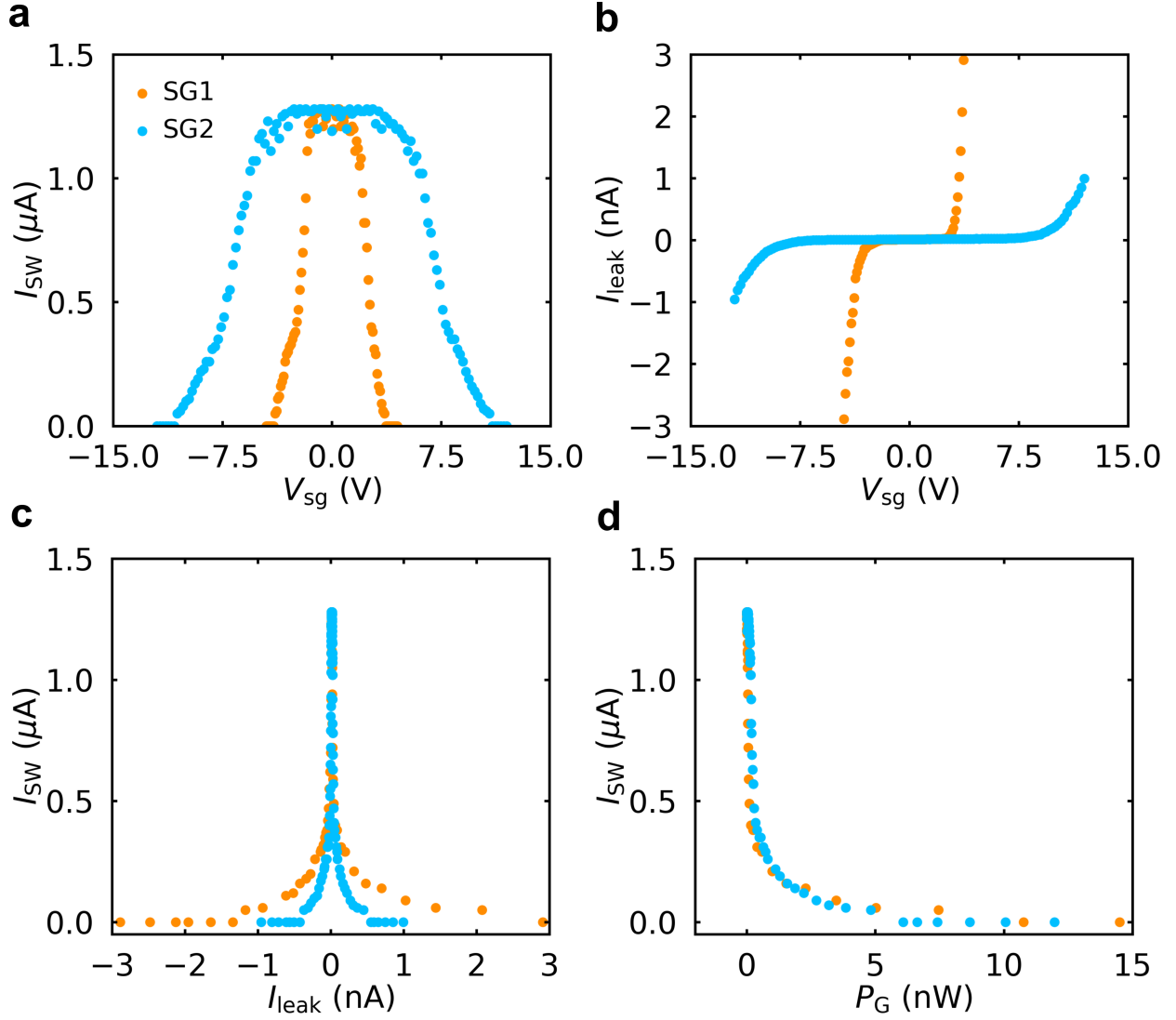


SFig. 5. **a** Parametric curve between I_{SW} and I_{leak} for SG1 (orange curve) and for SG2 (light blue) of device A. **b** I_{SW} as a function of P_G for both gates. The inset show a false colored SEM image for the investigated device with two opposite side gates colored same as their corresponding curves.

VI. INVESTIGATION OF DEVICE A IN ANOTHER COOLDOWN

By Investigating device A in another cool-down, the gate dependence of I_{SW} (see SFig. 6a) under the influence of SG1 (orange curve) and SG2 (light curve) gives an opposite situation to that obtained in the first cool-down (see Fig.1d,e in the main text). In this cool-down,

SG1 suppresses I_{SW} at lower V_{th} and $V_{sg,C}$ than SG2. On the other hand, a corresponding increase in I_{leak} is observed at V_{th} for the two gates (see SFig. 6b).

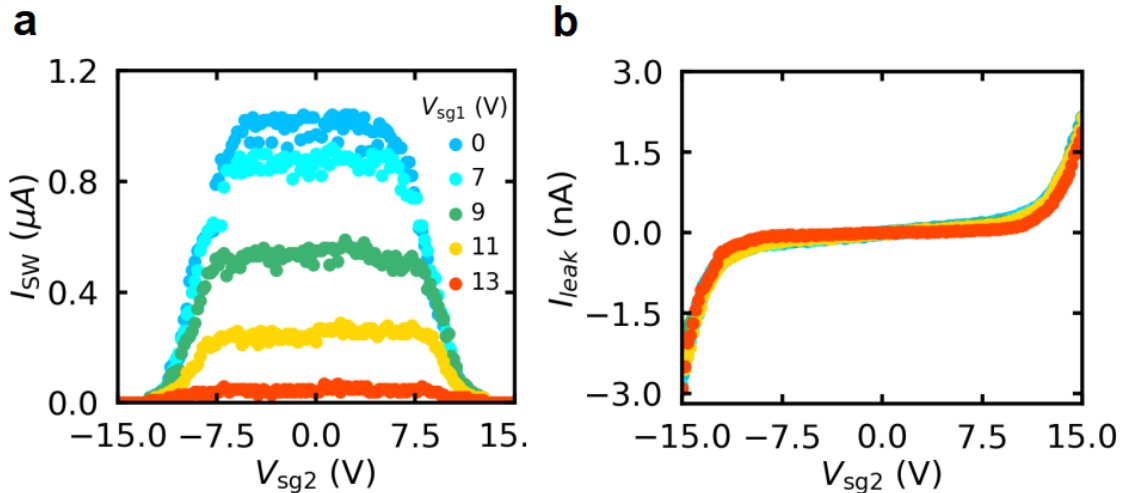


SFig. 6. **a** I_{SW} as a function of V_{sg} for SG1 (orange curve) and for SG2 (light blue curve) of device A in another cool-down. **b** I_{leak} as a function of V_{sg} for both gates. **c** Parametric curve between I_{SW} and I_{leak} . **d** I_{SW} as a function of P_G for both gates.

As in the previous section, plotting a parametric curve between I_{SW} and I_{leak} (see SFig. 6c) for the two gates shows that I_{SW} is suppressed at the onset of I_{leak} . Moreover, a strong matching between the influence of the two gates is obtained when I_{SW} is plotted as a function of P_G , as shown in SFig. 6d.

VII. DUAL-GATE MEASUREMENT

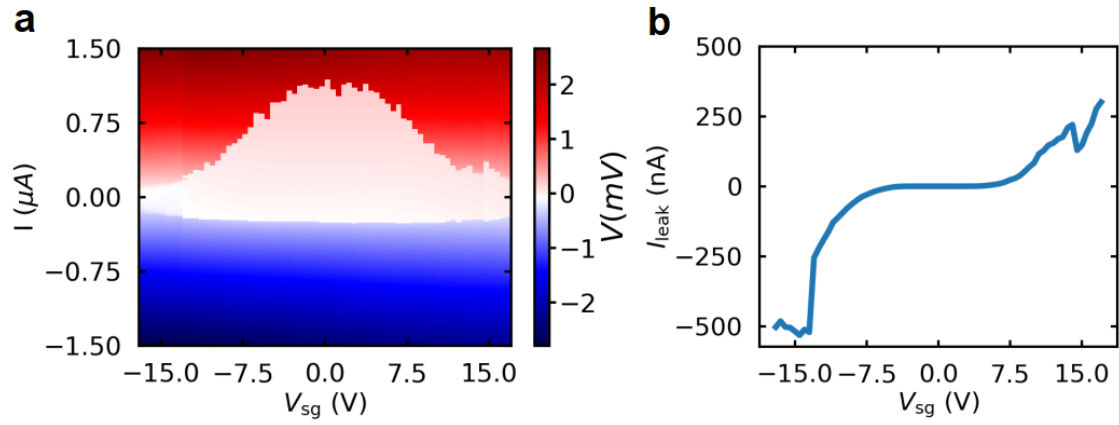
In this section, we will examine the effect of the two opposite side gates on the suppression of I_{SW} as well as on $V_{sg,C}$. SFig. 7a shows I_{SW} as a function of V_{sg2} at different values of V_{sg1} . For $V_{sg2} = 0$ V, I_{SW} decreases as expected with increasing V_{sg1} , while with increasing V_{sg2} , the dependence of I_{SW} on V_{sg2} looks quite similar for all values of V_{sg1} and no change in $V_{sg2,C}$ is observed. The independence $V_{sg,C}$ for one of the gates from the influence of the other has already been reported in Ref. ? , where the electric field was proposed as the origin of the gating effect. However, in our case a corresponding increase in the leakage current was observed as shown SFig. 7b.



SFig. 7. **a** I_{SW} and I_{leak} as a function of V_{sg2} at different values of V_{sg1} for device A **b** The corresponding V_{sg} versus I_{leak} .

VIII. MEASUREMENTS ON DIFFERENT SUBSTRATE

We have investigated the GCS in another Ta/InAs nanowire device with the same device configurations but fabricated on a sapphire substrate. Despite I_{SW} is not fully suppressed by V_{sg} in the ± 17 V window (see SFig. 8a), the corresponding I_{leak} (see SFig. 8b) and thus P_G is two orders of magnitude higher than for the devices fabricated on Si^{++}/SiO_2 substrate shown in the main text. A possible reason could be that in case of a phonon mediated scenario the different type of the substrates allow different phonon generation.



SFig. 8. **a** $I - V$ curve as a function of $\pm V_{\text{sg}}$ of a Ta/InAs nanowire device fabricated on a sapphire substrate. **b** The corresponding I_{leak} as a function of $\pm V_{\text{sg}}$.